removed and the solution filtered, reduced in volume, and cooled to give a pink-purple solid (0.115 g, 24%), which was washed and dried in vacuo; IR 1975, 1890, 1645, 1030, 960, 750, 395. Anal. Calcd for $C_{15}H_{25}ClO_2PTa$: C, 27.17; H, 5.20; Ta, 37.33. Found: C, 26.97; H, 5.22; Ta, 37.50.

Cp*Ta(dmpe)$H_2(C_2H_4)$ (18). A thick-walled quartz reaction vessel with a Teflon needle valve, charged with 0.90 g of **7**, 15 mL of benzene, and 5 mmol of ethylene (2 atm), was photolyzed while stirring for 3 days. A light yellow solid (0.50 g, 53%) was crystallized from benzene, washed with cold petroleum ether, and dried in vacuo; IR 1695, 1590, 1290, 1280, 1090, 1030, 940, 925, 892, 840, 790, 740, 720, 695, 650. Anal. Calcd for $C_{18}H_{37}P_2Ta$: C, 43.55; H, 7.51; Ta, 36.45. Found: C, 43.34; H, 7.32; Ta, 36.74.

Cp*TaCH$_2$CH$_2$CH$_2$CH$_2$(C_4H_6) (19). **19** has been prepared by another route and characterized by Schrock and co-workers.[37] A thick-walled glass reaction vessel with a Teflon needle valve, charged with 0.83 g of **4**, 30 mL of petroleum ether, and 25 mmol of ethylene, was stirred for 6 h. **19** (0.12 g, 16%) was crystallized from the solution and dried in vacuo; IR 1040, 1030, 950, 845, 720.

Acknowledgment. This work has been supported by the National Science Foundation (Grant No. CHE-8024869). We also acknowledge use of the Southern California Regional NMR Facility and the support of NSF Grant No. 7916324A1.

Registry No. 2, 69302-75-6; **3**, 71763-35-4; **4**, 80964-80-3; **5**, 80964-81-4; **6**, 80964-82-5; **7**, 80964-83-6; **8**, 80964-84-7; **9**, 80964-85-8; **10**, 80975-59-3; **11**, 80964-86-9; **12**, 80964-87-0; **13**, 80964-88-1; **14**, 80964-89-2; **15**, 80964-90-5; **16**, 80964-91-6; **17**, 80964-92-7; **18**, 80964-93-8; **19**, 71860-93-0; Cp*Ta$(OCHMe_2)_4$, 80964-94-9; Cp*Ta$(OCHMe_2)_3$Cl, 80964-95-0; acetone, 67-64-1.

(37) (a) Fellmann, J. D.; Schrock, R. R.; Rupprecht, G. A. *J. Am. Chem. Soc.* **1981**, *103*, 5752–5758. (b) McLain, S. J. Ph.D. Thesis, Massachusetts Institute of Technology, 1979. (c) McLain, S. J., personal communication, 1982.

(38) Harris, R. K. *Can. J. Chem.* **1964**, *42*, 2275–2281. Leyden, D. E.; Cox, R. H. "Analytical Applications of NMR"; Wiley: New York, 1977; pp 104–109.

(39) Yasuda, H.; Kajihara, Y.; Mashima, K.; Nagasuna, K.; Lee, K.; Nakamura, A. *Ogranometallics* **1982**, *1*, 388–396.

(40) Bunker, M. J.; Green, M. L. H. *J. Chem. Soc., Dalton Trans.* **1981**, 85–90.

(41) Redfield, D. A.; Nelson, J. H.; Cary, L. W. *Inorg. Nucl. Chem. Lett.* **1974**, *10*, 727.

Synthesis, Crystal Structure and Molecular Conformations, and Magnetic Properties of a Cu^{II}–VO^{II} Heterobinuclear Complex: Interaction between Orthogonal Magnetic Orbitals

O. Kahn,*[1a] J. Galy,*[1b] Y. Journaux,[1a] J. Jaud,[1b] and I. Morgenstern-Badarau[1a]

Contribution from the Laboratoire de Spectrochimie des Elêments de Transition, ERA 672, Universitê de Paris Sud, 91405 Orsay, France, and the Laboratoire de Chimie de Coordination, Toulouse, France. *Received May 14, 1981*

Abstract: The complex $CuVO(fsa)_2en\cdot CH_3OH$, where $(fsa)_2en^{4-}$ denotes the binucleating ligand derived from the Schiff base *N,N'*-(2-hydroxy-3-carboxybenzylidene)-1,2-diaminoethane, has been synthesized and its crystal structure solved at room temperature. It crystallizes in the monoclinic system, space group $P2_1/n$. The lattice constants are $a = 11.636$ (3) Å, $b = 13.612$ (3) Å, $c = 12.426$ (3) Å, and $\beta = 100.8$ (4)° with $Z = 4$. Least-squares refinement of the structure led to a conventional weighted R factor of 0.082. The structure is made of heterobinuclear units, in which a copper atom is fivefold coordinated to two nitrogens, two phenolic oxygens, and the oxygen of a methanol molecule, and a vanadium atom is also fivefold coordinated to two phenolic and two carboxylic oxygens and the oxygen of the vanadyl group. At the accuracy of the experimental results, the metallic atoms and the oxygens of the methanol molecule and of the vanadyl group are in a mirror plane σ for the two square-pyramids CuN_2O_3 and VO_5. These pyramids point in the same direction. During the crystal growing attempts, in addition to the compound described above (**1**), species **2** and **3** were detected. **2** is built up from molecules with CuN_2O_3 and VO_5 pyramids orientated up–up and up–down in the respective proportions of 80% and 20% and randomly distributed within the crystal. **3** consists of a random distribution of molecules with conformation close to **1** and molecules of $Cu_2(fsa)_2en\cdot CH_3OH$ following the proportion of 85% and 15%, respectively. The magnetic behavior of **1** studied in the temperature range 4–300 K reveals an intramolecular ferromagnetic coupling characterized by a ground triplet state separated by around $J = 118$ cm^{-1} from the excited singlet state. The EPR spectrum confirms that the triplet state is the lowest and is interpreted with a zero-field splitting characterized by $|D| = 0.24$ cm^{-1} and $E = 0.04$ cm^{-1}. The nature of the intramolecular interaction is easily explained by the orthogonality of the magnetic orbitals centered on the Cu(II) and V(IV) metallic ions, antisymmetric and symmetric, respectively, with regard to the mirror plane σ. The magnitude of the ferromagnetic interaction may be interpreted from considerations of overlap density between the magnetic orbitals. In the present case, the overlap density map exhibits two strongly positive lobes around one of the oxygen bridges and two strongly negative lobes around the other oxygen bridge. Finally, a strategy is proposed to obtain new binuclear complexes exhibiting a strong ferromagnetic coupling with binucleating ligands of the same type as $(fsa)_2en^{4-}$.

In a communication published 3 years ago,[2] we described the synthesis and the main structural parameters of the heterobinuclear complex $CuVO(fsa)_2en\cdot CH_3OH$, where $(fsa)_2en^{4-}$ stands for the heterobichelating ligand derived from the Schiff base *N,N'*-(2-hydroxy-3-carboxybenzylidene)-1,2-diaminoethane. The interest of this complex, in our opinion, lies in the fact that the exchange interaction between Cu^{II} and VO^{II} ions is purely ferromagnetic due to the orthogonality of the magnetic orbitals ϕ_{Cu} and ϕ_{VO} centered on the Cu^{II} and V^{IV} ions, respectively. To the best of our knowledge, $CuVO(fsa)_2en\cdot CH_3OH$ was one of the first complexes exhibiting this property.[3] Since this communication, the

(1) (a) Laboratoire de Spectrochimie des Elêments de Transition. (b) Laboratoire de Chimie de Coordination.

(2) Kahn, O.; Galy, J.; Tola, P.; Coudanne, H. *J. Am. Chem. Soc.* **1978**, *100*, 3931–3933.

(3) To the best of our knowledge, the Cu^{II}–VO^{II} complexes described up to now have not been characterized structurally. For instance, see: Selbin, J.; Ganguly, L. *Inorg. Nucl. Chem. Lett.* **1969**, *5*, 815–818. Okawa, H.; Kida, S. *Inorg. Chim. Acta* **1977**, *23*, 253–257. Fenton, D. E.; Gayda, S. E. *J. Chem. Soc., Dalton Trans.* **1977**, 2109–2115.

0002-7863/82/1504-2165$01.25/0

work was pursued in three directions: (i) We have looked for a synthesis less aleatory and leading to a better yield than that described in ref 2. At the same time, we have multiplied the attempts to obtain single crystals suitable for a complete structural study. (ii) We have tried to determine the crystal structure of the complex as accurately as possible, in spite of the numerous technical difficulties related to the nature of the compound. Indeed, if the main structural parameters have been known since 1978 sufficiently well to specify the molecular arrangement, the full refinement of the structure would not have been possible because of the low quality of the available crystals. During the crystal growing attempts, we have obtained in addition to the species $CuVO(fsa)_2en\cdot CH_3OH$ ordered, succinctly described in ref 2 and designated **1**, two new species, namely, $CuVO(fsa)_2en\cdot CH_3OH$ disordered, **2**, where the disorder involves the vanadyl group and $Cu(VO)_{0.85}Cu_{0.15}(fsa)_2en\cdot CH_3OH$, **3**. In the present paper, we shall also briefly recall[4] the structure of **4**, $Cu_2(fsa)_2en\cdot CH_3OH$, for two reasons: first, the structures of $CuVO(fsa)_2en\cdot CH_3OH$ and $Cu_2(fsa)_2en\cdot CH_3OH$ are intimately related; second, we shall compare, from both experimental and theoretical points of view, the magnetic properties of the two complexes. (iii) We have sought to investigate thoroughly the mechanism of exchange in the Cu^{II}–VO^{II} pair. The thermal variation of the magnetic susceptibility of **1** shows without any ambiguity that the ground level is a spin triplet separated by about 118 cm^{-1} from a spin singlet and thus that the intramolecular coupling is ferromagnetic. The EPR spectrum confirms the existence of a ground triplet state. Even if the orthogonality of the magnetic orbitals can fully explain why the coupling is ferromagnetic, this fact alone cannot explain why the triplet–singlet energy gap is found to be so large. The next to the last part of this paper will deal with an approach of the exchange interaction based on the concept of overlap density between magnetic orbitals, which will justify the magnitude of the ferromagnetic interaction in **1**. Finally, by way of conclusion, we shall give the broad outline of a strategy to synthesize new coupled systems exhibiting strong ferromagnetic coupling.

In the last few years, several papers were devoted to the synthesis, the determination of the structures, and the study of the magnetic properties of heterobimetallic complex.[5-15] The goal of this work is not only to describe in detail a new complex belonging to this class of compounds but, more specially, to focus on the phenomenon of orthogonality of the magnetic orbitals and on the design of strongly ferromagnetically coupled systems.

Experimental Section

Syntheses. The preparation of **1** giving the best yield was as follows: $CuH_2(fsa)_2en\cdot 0.5H_2O$ and $VO(CH_3COO)_2$ were first synthesized by using the described procedures.[16,17] $CuH_2(fsa)_2en\cdot 0.5H_2O$ (200 mg) (4.7×10^{-4} mol) was stirred with 37.5 mg of NaOH (9.4×10^{-4} mol) in 150 mL of methanol. Then 37.5 mg of $VO(CH_3COO)_2$ (4.7×10^{-4} mol) was introduced in an extractor cartridge above the methanolic solution. This solution was heated at reflux for 24 h until complete dissolution of $VO(CH_3COO)_2$ had occurred. **1** precipated as dark blue polycrystalline powder. It was separated by filtration, washed with methanol, and dried under reduced pressure. All the operations were carried out under nitrogen atmosphere. Anal. Calcd for $C_{19}H_{16}N_2O_7CuV$: C, 44.33; H, 3.13; N 5.44. Found: C, 43.86; H, 3.23; N, 5.35. An X-ray powder diagram confirmed that the compound was actually **1**, the structure of which is described below. The infrared spectrum exhibits an intense band characteristic of the V–O stretching vibration at 995 cm^{-1}. The yield of the method is quantitative, but we were unable to obtain single crystals suitable for X-ray study.

An alternative preparation of **1**, giving very small crystals eventually suitable for X-ray work, consisted of reacting $CuH_2(fsa)_2en\cdot 0.5H_2O$ with $VO(OH)_2$.[18] Each compound was introduced in stoichiometric amount in a filter paper cartridge. The two cartridges were immersed in deoxygenated methanol under nitrogen atmosphere. After several weeks, crystals appeared on the cartridge containing primitively $CuH_2(fsa)_2en\cdot 0.5H_2O$. Most of them corresponded to **1**. In some attempts, we detected crystals of **2**.

The best way to obtain single crystals of **1** is that described in ref 2. A solution of lithium salt of $CuH_2(fsa)_2en\cdot 0.5H_2O$ was prepared by stirring together 10^{-4} mol of this complex with 2×10^{-4} mol of $LiOH\cdot H_2O$ in 80 mL of methanol. To this solution was slowly added a solution of 10^{-4} mol of $VOSO_4\cdot 5H_2O$ in 40 mL of methanol. About 0.6×10^{-4} mol of $CuH_2(fsa)_2en\cdot 0.5H_2O$ reprecipitated. The mixture was then filtered and the resulting blue solution kept in a flask closed under nitrogen. Dark blue single crystals of **1** appeared within 1 or 2 days. In some attempts, single crystals of **3** were detected.

X-ray Analysis. Structure Determination. During the crystal growth experiments, a real difficulty was noticed in selecting suitable crystals for X-ray analysis; indeed, in spite of rather well-formed single crystals, the data collections were made particularly tedious owing to their poor diffractory power. Moreover, the crystals were also rather quickly destroyed by a kind of efflorescing process. In order to protect them somewhat, we mounted the crystals in Lindeman glass capillaries. After a very large number of attempts to select crystals of good quality, it became clear to us that three species actually did exist: **1**, **2**, and **3** as noted above.

The preliminary X-ray studies were conducted by photographic methods using a Weissenberg camera (Ni-filtered Cu Kα radiation) or an Explorer camera (Zr-filtered Mo Kα radiation). The density measurements were performed by the flotation method. Intensity data were collected at room temperature on a CAD 4 Enraf-Nonius PDP8/M computer-controlled single-crystal diffractometer. All the information concerning crystallographic data collections and results are summarized in Table I. The unit cell parameters have been refined by optimizing the settings of 25 reflections. The intensity of the utilized reflections $|I > \sigma(I)|$ was corrected for Lorentz and polarization factor. For crystals of **2** and **3** measured with molybdenum radiation, the intensity was not corrected from absorption ($\mu\bar{r} \simeq 0.8$). For **1** measured with copper radiation, a spherical absorption correction was applied, justified by the regular faceted block appearance of the crystal ($\mu\bar{r} \simeq 1.2$). Atomic scattering factors of Cromer and Weber[19] for the nonhydrogen atoms and Simpson[20] for the spherical hydrogen atoms were used. Real and imaginary dispersion corrections given by Cromer were applied for copper and vanadium atoms.

Direct methods were used to solve the structural problems (MULTAN 7). In a first step, the program yielded the positions of the heavy atoms (Cu(1) and V) and their immediate surroundings; the carbon and oxygen atoms of the ligand were located by Fourier synthesis. The structure was then refined by combining full-matrix least-squares techniques and difference Fourier maps. This last technique associated with a priori calculations made it possible for the positions of hydrogen atoms to be determined. All nonhydrogen atoms were then allowed to refine with isotropic thermal parameters of $B_H = 1.2\ B_{iC}$ (B_{iC} is the equivalent isotropic temperature factor of the carbon to which the hydrogen is bonded; $B_{iC} = {}^4/_3 \sum_{i,j}(\bar{a}_i\bar{a}_j)\beta_{ij}$). Final difference Fourier maps show the highest residual peaks near the metal position at a level lower than 0.7 e/Å^3. Atomic coordinates and thermal factors for all nonhydrogen atoms pertaining to the structures **1**, **2**, and **3** are given in Table II. The same information for **4** was given in ref 4.

Magnetic Measurements. The magnetic measurements were carried out on polycrystalline samples of compound **1** weighing about 8 mg in

(4) Galy, J.; Jaud, J.; Kahn, O.; Tola, P. *Inorg. Chim. Acta* **1979**, *36*, 229–236.
(5) Glick, M. D.; Lintvedt, R. L.; Anderson, T. J.; Mack, J. L. *Inorg. Chem.* **1976**, *15*, 2258–2262, and references therein.
(6) Groh, S. E.; *Isr. J. Chem.* **1976**, *15*, 277–307, and references therein.
(7) Okawa, H.; Nishida, Y.; Tanaka, M.; Kida, S. *Bull. Chem. Soc. Jpn.* **1977**, *50*, 127–131 and references therein.
(8) Mikuriya, M.; Okawa, H.; Kida, S.; Ueda, I. *Bull. Chem. Soc. Jpn.* **1978**, *51*, 2920–2923.
(9) Beale, J. P.; Cunningham, J. A.; Phillips, D. J.; *Inorg. Chim. Acta* **1979**, *33*, 113–118.
(10) Graziani, R.; Vidali, M.; Rizzardi, G.; Casellato, U.; Vigato, P. A. *Inorg. Chim. Acta* **1979**, *36*, 145–150 and references therein.
(11) Casellato, U.; Vigato, P. A.; Fenton, D. E.; Vidali, M. *Chem. Soc. Rev.* **1979**, *8*, 199–220.
(12) Leslie, K. E.; Drago, R. S.; Stucky, G. D.; Kitko, D. J.; Breese, J. A. *Inorg. Chem.* **1979**, *18*, 1885–1891.
(13) O'Connor, C. J.; Freyberg, D. P.; Sinn, E. *Inorg. Chem.* **1979**, *18*, 1077–1088.
(14) Galy, J.; Jaud, J.; Kahn, O.; Tola, P. *Inorg. Chem.* **1980**, *19*, 2945–2948 and references therein.
(15) Jaud, J.; Journaux, Y.; Galy, J.; Kahn, O. *Nouv. J. Chim.* **1980**, *4*, 629–630.
(16) Tanaka, M.; Kitaoka, M.; Okawa, H.; Kida, S. *Bull. Chem. Soc. Jpn.* **1976**, *49*, 2469–2473.
(17) Paul, R. C.; Bhatia, S.; Kumar, A. *Inorg. Synth.* **1972**, *13*, 181–183.
(18) Morette, A. *C.R. Hebd. Seances Acad. Sci. Ser. B* **1950**, *231*, 408–410.
(19) Cromer, D. T.; Waber, J. T. *Acta Crystallogr.* **1965**, *18*, 104–109.
(20) Stewart, R. F.; Davidson, E. R.; Simpson, W. T. *J. Chem. Phys.* **1965**, *42*, 3175–3187.

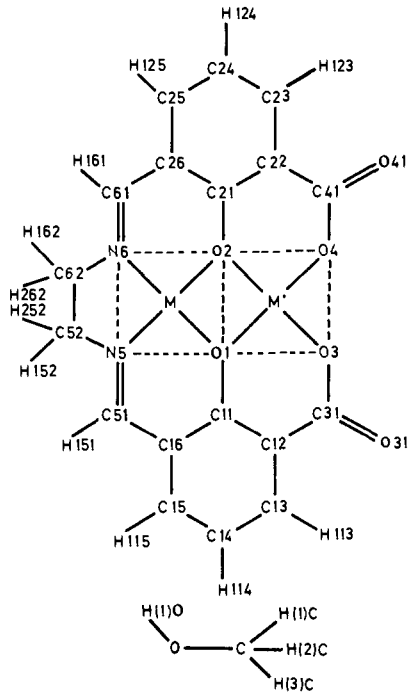

Figure 1. Schematic drawing and labeling of the atoms for MM'-$(fsa)_2en{\cdot}CH_3OH$.

the temperature range 3.8–300 K with a Faraday type magnetometer equipped with a continuous flow cryostat. The applied magnetic field was about 0.6 T. The independence of the susceptibility against the magnetic field was checked at both room temperature and 20 K. Mercuritetrakis(thiocyanato)cobaltate was used as susceptibility standard. The uncertainty on the temperature is about 0.1 K and on the susceptibility about 30×10^{-6} cm^3 mol^{-1}. The diamagnetism was estimated as -280×10^{-6} cm^3 mol^{-1}.

EPR Measurements. The EPR study was carried out on a powdered sample in the 4.2–300-K temperature range with a Bruker X-band ER 20 spectrometer equipped with a continuous flow cryostat. Field modulation (100 kHz) was used, and the magnetic fields were measured by a Hall probe.

Description of the Structures

A schematic drawing of the whole molecule with metallic sites indicated by M and M' and labeling of the carbon, nitrogen, oxygen, and hydrogen atoms together with the methanol molecule is indicated in Figure 1. A perspective view of molecule **1** without hydrogen atoms is given in Figure 2. The main bond lengths and bond angles for compounds **1**–**4** are listed in Table IIIa,b.

General Description of the Molecule. In the binuclear complex $MM'(fsa)_2en{\cdot}CH_3OH$, the inside site M is occupied by the copper atom Cu(1) in compounds **1**–**4**. A methanol molecule is weakly bound to this copper. The outside site M' is occupied by VO^{II} in **1**, disordered VO^{II} in **2**, Cu^{II} and VO^{II} in **3** with roughly 15% of copper and 85% of vanadyl, and Cu^{II} in **4**. The details of the ligand have been obtained with a good accuracy in **4**, and the data concerning bond lengths and bond angles of **1**, **2**, and **3** are in reasonably good agreement and warrant no additional comment here.

Molecular Packing. Compounds **1**, **2**, and **3** pack in a similar way in the crystal unit cell. The molecules pile up along the plane ($\bar{1}01$), the pseudotwofold axis MM' of the molecule $MM'(fsa)_2en$ being almost parallel with the direction (301). The "barycenter" of the molecule, located between M and M' very close to the ($\bar{1}01$) plane, alternates with the symmetry centers and helicoidal twofold axis of the cell. This can be readily seen in Figure 3a, which is a projection onto the (010) plane of the molecular skeleton $CuVO(N_2O_4){\cdot}CH_3OH$ together with the symmetry elements.

The main difference with the molecular packing encountered in **4** (Figure 3b) lies in the fact that the pseudotwofold axis is then parallel to the direction (302) and that the "barycenter" alternates with the symmetry elements along the (101) plane even though

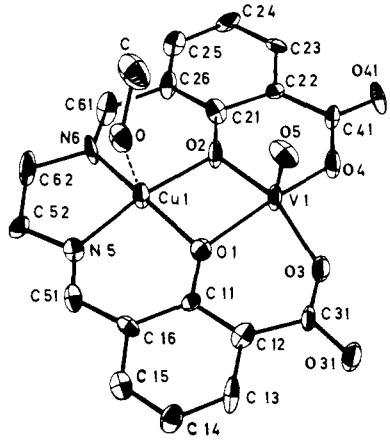

Figure 2. Perspective view of compound **1**, $CuVO(fsa)_2en{\cdot}CH_3OH$.

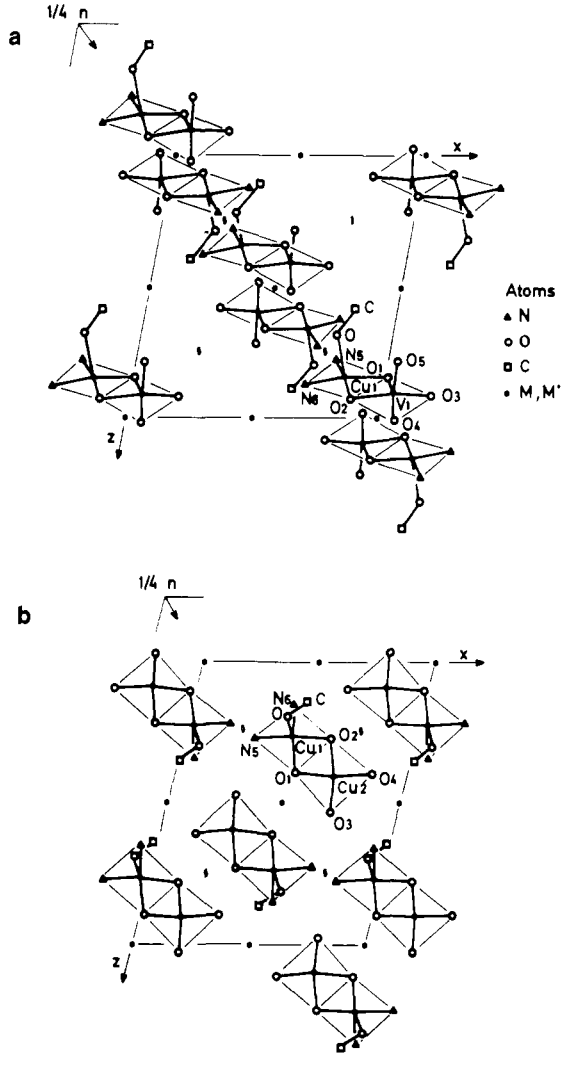

Figure 3. Comparison of the molecular packing for **1** (a) and **4** (b).

there is a remarkable vicinity of crystallographic data between **1** and **4**. Note that the molecules **1**, **2**, and **3** are very close to a symmetry center (the molecule of reference; positions indicated in Table II are close to the center 111); we shall see further the difficulties arising from this structural feature.

Detailed Molecular Features. In **1**, **2**, and **3**, the inside site M is fully occupied by a copper atom. This Cu(1) atom is fivefold coordinated in a square pyramid to two nitrogen atoms [N(5) and N(6)], two phenolic oxygen atoms [O(1) and O(2)], and the oxygen atom (O) of the methanol molecule occupying the apex of the pyramid. The length of the Cu(1)–O bond, around 2.3 Å,

Table I. Information Concerning Crystallographic Data Collections for 1, 2, 3, and 4

	1	2	3	4
	1. Crystallographic and Physical Data			
formula	$CuVO\ O_7N_2C_{19}H_{16}$	$CuVO\ O_7N_2C_{19}H_{16}$ (VO ordered 80%)	$CuCu_{0.15}(VO)_{0.85}O_7N_2C_{17}H_{16}$	$CuCu\ O_7N_2C_{19}H_{16}$
crystal system	monoclinic	monoclinic	monoclinic	monoclinic
a, Å	11.636 (3)	11.629 (5)	11.613 (4)	11.456 (5)
b, Å	13.612 (3)	13.579 (5)	13.533 (6)	11.425 (3)
c, Å	12.426 (3)	12.416 (4)	12.314 (5)	14.357 (4)
β, deg	100.8 (4)	101.2 (5)	101.0 (5)	104.2 (3)
molecular weight	514.48	514.48	513.80	511.30
space group	$P2_1/n$	$P2_1/n$	$P2_1/n$	$P2_1/n$
V, Å^3	1933	1923	1899	1822
Z	4	4	4	4
$F(000)$	1040	1040	1038.4	1036
ρ_{exptl}, g/cm^3	1.78 (5)	1.77 (5)	1.81 (5)	1.89 (2)
ρ_x, g/cm^3	1.752	1.785	1.805	1.87
absorption factor, cm^{-1}	61.0 (Cu Kα)	17.1 (Mo Kα)	18.7 (Mo Kα)	24.4 (Mo Kα)
morphology: cm (max and min size) little regular bloks	0.040-0.038	0.042-0.040	0.048-0.038	0.028-0.022
	2. Data Collection			
temp, °C	21	20	20	20
radiation	Cu Kα	Mo Kα	Mo Kα	Mo Kα
monochromatisation: monochromator graphite λ Kα	1.5418 Å	0.71069	0.71069	0.71069
crystal-detector distance, mm	207	207	207	207
detector windows: height,[a] mm	4	4	4	4
width,[a] mm	3.20 + 0.70$tg\theta$	4	3.80 + 0.90$tg\theta$	1.8 + 3.5$tg\theta$
take-off angle,[a] deg	6.5	4	5.5	4.25
scan mode	$\theta/2\theta$	$\theta/2\theta$	$\theta/2\theta$	$\theta/2\theta$
maximum Bragg angle, deg	50	26	30	30
scan angle for ω angle	1. + 0.142$tg\theta$	0.80 + 0.347$tg\theta$	0.67 + 0.347$tg\theta$	0.85 + 0.35$tg\theta$
values determining the scan speed				
Sigpre[a]	0.4	0.75	0.45	0.4
Sigma[a]	0.018	0.018	0.018	0.018
Vpre[a] deg/mm	10	10	10	10
Tmax[a] s	50	80	95	90
controls:				
reflections	600, 033, 220	01$\bar{1}$, 02$\bar{3}$, 01$\bar{3}$	600, 042, 136	$\bar{4}42$, $\bar{3}05$, 600
intensity periodicity, 3600 s				
orientation after 100 reflections		032, $\bar{2}3\bar{6}$, $2\bar{1}\bar{5}$	046, 662, 171	$\bar{4}52$, 413, $\bar{6}00$
	3. Conditions for Refinement			
reflections for the refinement of the cell dimensions:	25	25	25	25
recorded reflections	2115	4212	5396	4541
independent reflections: obsd	1428	1905	1612	3830
utilized reflections $I > \sigma(I)$	1278	1670	1476	2958
refined parameters:	280	289	284	272
reliability factors:				
$R = \Sigma\|kF_o - \|F_c\|\|/\Sigma kF_o$	0.082	0.069	0.073	0.043
$R_w = [\Sigma(kF_o - \|F_c\|)^2/\Sigma wk^2F_o^2]^{1/2}$	0.086	0.073	0.091	0.052

[a] These parameters have been described by: Mosset, X. X.; Bennet, J.; Galy, J. *Acta Crystallogr. Sect. B* 1977, *B33*, 2639.

shows that the Cu(1)–methanol interaction is strong enough to pull the copper atom out of the mean plane O(1)O(2)N(5)N(6) by around 0.2 Å (see Table IV). As far as the outside site M′ is concerned, the three species must be discussed separately.

Compound 1. The vanadyl group is grafted in a classical way onto the square plane O(1)O(2)O(3)O(4) formed by the two phenolic and two carboxylic oxygen atoms. The two pyramids Cu(1)ON(5)N(6)O(1)O(2) and V(1)O(5)O(1)O(2)O(3)O(4) share the edge O(1)O(2) and are pointing in the same direction. This is rather unusual, generally square pyramids sharing edges being up and down.[21]

The square planes of the pyramids make a dihedral angle of 190°, this fact being explained by the repulsion between the apexes occupied by oxygen atoms O and O(5) of the methanol molecule and the vanadyl group, respectively. O(5) repulses also the methyl group, as indicated by the dihedral angle between Cu(1)OC and OCu(1)V(1), the CH_3 group being able to rotate around the Cu(1)–O bond. This angle is about 20° larger in **1** (75°) than in **4** (56°). At the accuracy of the experimental results, the atoms O(5), V(1), Cu(1), and O are in a mirror plane for both CuN_2O_3 and VO_5 square pyramids (see Table IV).

Compound 2. A reasonably accurate refinement of the structure of **2** was rather difficult. Anyhow, the most important features have been obtained and are reported in this paper. During the refinement process of the crystal structure, the increase of the thermal parameters of the vanadyl group |V(1)O(5)| and the presence in the difference Fourier maps of smeared electron density "below" the plane O(1)O(2)O(3)O(4), CH_3OH and V(1)O(5) being "above" this plane, gave a strong evidence for the presence of some vanadyl groups in the position V(D1)O(D5). The refinement was then pursued by introducing this new molecular conformation with the two square pyramids Cu(1)ON(5)N(6)-O(1)O(2) and V(D1)O(D5)O(1)O(2)O(3)O(4) up and down, respectively (see Figure 4 a and b). The main difficulty for the V(D1)O(D5) group to be properly refined comes from the vicinity in the cell of the neighbor molecule (obtained by the repetition

(21) Bouloux, J. C.; Galy, J. *J. Solid State Chem.* **1976**, *16*, 385–391.

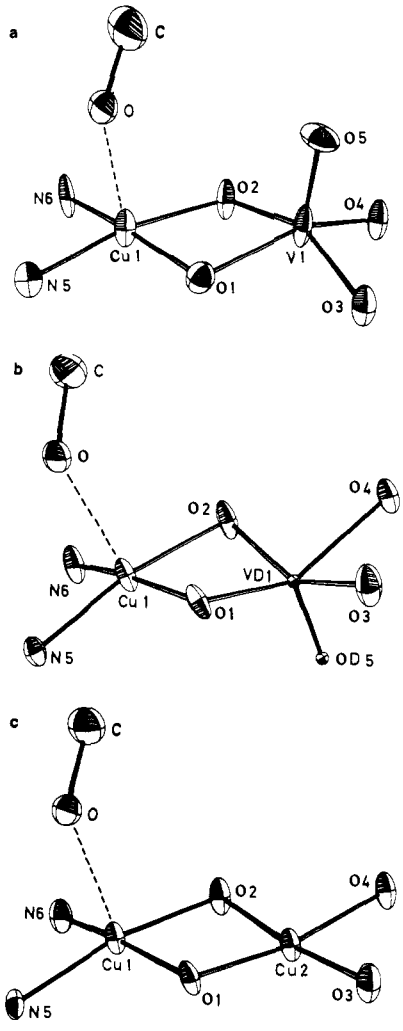

Figure 4. (a) Perspective view of $CuVO(fsa)_2en{\cdot}CH_3OH$ with CuN_2O_3 and VO_5 pyramids pointing in the same direction. (b) Perspective view of $CuVO(fsa)_2en{\cdot}CH_3OH$ with CuN_2O_3 and VO_5 pyramids pointing up–down. (c) Perspective view of $Cu_2(fsa)_2en{\cdot}CH_3OH$ (see text).

of the cell through the inversion with regard to the crystallographic symmetry center) which squeezes this group. Anyhow, the final R factor, 0.069, the value of the thermal parameters, and the final difference Fourier maps exhibiting peaks lower than 0.8 e/Å^3 justify the description of the crystal structure as being built up from molecules having conformations illustrated in Figure 4 a and b, in the respective proportions of 80% and 20% and randomly distributed within the crystal. It can be noticed from Table IIIa that the distances V(1)–O(5) and V(D1)–O(D5) in **2** are in correct agreement with the distance V(1)–O(5) in **1** and that the distances of the vanadium atoms from the square plane, around 0.5 Å, fit with the values generally observed for a V^{IV} in a square pyramid of oxygen atoms.[22]

Compound 3. Similar phenomena arose during the refinement of structure **3**. Some copper atoms appear to be substituted to vanadyl groups in the M′ site. The structure consists then in a random distribution of molecules with conformation close to **1** (Figure 4a) and of molecules $Cu_2(fsa)_2en{\cdot}CH_3OH$ (Figure 4c) with proportions of 85% and 15%, respectively.

Discussion of the Magnetic and EPR Data

The magnetic behavior of **1** is shown in Figure 5 under the form of the variation of $\chi_M T$ vs. the temperature T over the range $3.8 < T/K < 300$. χ_M being the molar magnetic susceptibility. Upon cooling from 300 K to around 50 K, $\chi_M T$ increases, then reaches

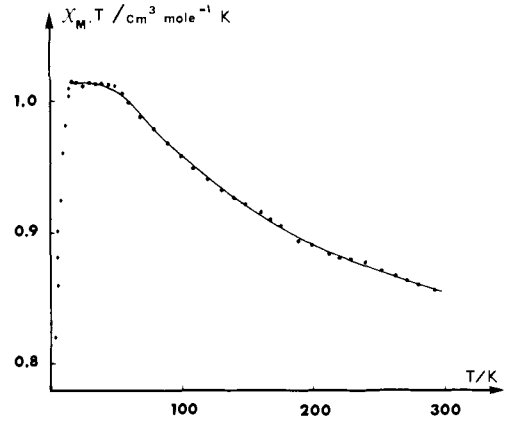

Figure 5. Experimental and theoretical temperature dependencies of the product $\chi_M T$ for **1**. The experimental points are noted ● and the theoretical curve is in a continuous line.

a maximum, and remains essentially constant down to 18 K, and finally decreases again below 18 K. The interpretation of the magnetic behavior in the range 18–300 K is straightforward. Both Cu^{II} and VO^{II} ions have an unpaired electron. The exchange interaction between the two single-ion spin doublets leads to two molecular levels characterized by $S = 0$ and $S = 1$, respectively, and separated by J. J is positive if the spin triplet is the lowest level. The increase of $\chi_M T$ upon cooling down shows that the $S = 1$ level is actually the lowest in energy. Below 50 K, the $S = 0$ level is totally depopulated so that $\chi_M T$ is constant. The variation of $\chi_M T$ below 18 K is most likely due to an intermolecular antiferromagnetic coupling between the $S = 1$ molecular spins.

If the spin Hamiltonian for the Cu^{II}–VO^{II} pair is written according to

$$\mathcal{H} = \beta(g_{Cu}\hat{S}_{z_{Cu}} + g_{VO}\hat{S}_{z_{VO}})\cdot\vec{H} - J\hat{S}_{Cu}\hat{S}_{VO}$$

where g_{Cu} and g_{VO} are the g factors for the metallic centers, assumed to be isotropic, and J is the singlet–triplet energy gap, then the theoretical expression for $\chi_M T$ is

$$\chi_M T = \frac{2N\beta^2 g^2}{k}\left[3 + \exp\left(-\frac{J}{kT}\right)\right]^{-1} + \left(\frac{2N\beta^2\delta^2 T}{J}\right)\left(\frac{1 - \exp\left(-\frac{J}{kT}\right)}{3 + \exp\left(-\frac{J}{kT}\right)}\right) + N\alpha$$

The constants N, β, and k and the parameter $N\alpha$ have their usual meaning. g and δ are defined as

$$g = \frac{g_{Cu} + g_{VO}}{2}$$

$$\delta = \frac{g_{Cu} - g_{VO}}{2}$$

The second term in the expression of $\chi_M T$ arises from the second-order coupling of the two $M_S = 0$ components associated to the $S = 1$ and $S = 0$ levels, respectively.[23] When the two interacting ions are equivalent, this term vanishes. In the present case, the second-order term is negligible, owing to the large singlet–triplet energy gap. Least-squares fitting procedure in the range 18–300 K led to $J = 118$ cm^{-1}, $g = 2.02$, and $N\alpha$ negligible. The agreement factor defined here as $\sum[(\chi_M T)_{obsd} - (\chi_M T)_{calcd}]^2/\sum[(\chi_M T)_{obsd}]^2$ is then equal to 0.5×10^{-4}.

The powder EPR spectrum of **1** measured at 100 K is shown in Figure 6. The thermal variation of the intensities in the temperature range 4.2–300 K confirms that all the features, except perhaps the broad peak around 4800 G, are associated with a

(22) Glick, M. D.; Lintvedt, R. L.; Gavel, D. P.; Tomlonovic, B. *Inorg. Chem.* **1976**, *15*, 1654–1660.

(23) Barraclough, C. G.; Brookes, R. W.; Martin, R. L. *Aust. J. Chem.* **1974**, *27*, 1843.

Table II. Atomic Coordinates and Thermal Factors for All Nonhydrogen Atoms of Structures 1, 2, and 3[a]

atom	x	y	z	U_{11} or B(A°)	U_{22}	U_{33}	U_{12}	U_{13}	U_{23}
				$CuVOO_7N_2C_{19}H_{16}$ (1)					
Cu(1)	0.8343 (2)	0.5470 (2)	0.8419 (3)	3.3 (2)	4.8 (2)	9.7 (3)	−0.5 (2)	0.8 (2)	−1.7 (2)
V(1)	1.0402 (4)	0.6817 (4)	0.8934 (5)	1.9 (2)	7.6 (4)	11.2 (5)	−0.7 (3)	0.7 (3)	−4.6 (4)
N(5)	0.683 (1)	0.539 (1)	0.877 (2)	4. (1)	3. (1)	8. (1)	0.9 (10)	1. (1)	−1. (1)
N(6)	0.807 (1)	0.423 (1)	0.777 (2)	2.1 (9)	7. (1)	14. (2)	−1. (1)	3. (1)	−3. (1)
O(1)	0.880 (1)	0.661 (1)	0.929 (1)	4.9 (9)	7. (1)	6. (1)	0.2 (8)	0.9 (9)	−1.1 (9)
O(2)	1.002 (1)	0.547 (1)	0.837 (1)	3.4 (8)	5. (1)	12. (1)	−1.6 (8)	1.1 (8)	−3.7 (10)
O(3)	1.059 (1)	0.769 (1)	1.015 (1)	3.8 (9)	7. (1)	10. (1)	−0.9 (9)	1.2 (9)	−3. (1)
O(4)	1.197 (1)	0.637 (1)	0.919 (1)	2.7 (8)	7. (1)	11. (1)	−0.7 (8)	0.2 (8)	−2. (1)
O(31)	1.027 (1)	0.886 (1)	1.124 (1)	4.4 (9)	9. (1)	12. (2)	−0.9 (10)	0.0 (10)	−5. (1)
O(41)	1.356 (1)	0.575 (1)	0.879 (1)	1.5 (8)	7. (1)	14. (2)	0.0 (7)	1.3 (8)	1. (1)
O	0.771 (1)	0.633 (1)	0.682 (1)	4.0 (9)	10. (1)	8. (1)	0.7 (9)	0.0 (8)	3. (1)
O(5)	1.028 (2)	0.753 (1)	0.792 (2)	6. (1)	11. (2)	7. (1)	2. (1)	2. (1)	5. (1)
C(11)	0.815 (2)	0.716 (2)	0.979 (2)	4. (1)	5. (2)	3. (1)	0. (1)	0. (1)	0. (1)
C(12)	0.865 (2)	0.797 (2)	1.036 (2)	6. (2)	5. (2)	6. (2)	1. (1)	−1. (1)	0. (1)
C(13)	0.791 (2)	0.859 (2)	1.088 (2)	5. (2)	6. (2)	12. (3)	−2. (1)	−2. (2)	0. (2)
C(14)	0.676 (2)	0.841 (2)	1.083 (2)	6. (2)	5. (2)	9. (2)	0. (1)	−1. (1)	−1. (1)
C(15)	0.630 (2)	0.757 (2)	1.031 (2)	5. (1)	5. (2)	6. (2)	1. (1)	0. (1)	3. (1)
C(16)	0.694 (2)	0.691 (2)	0.976 (2)	4. (1)	6. (2)	6. (2)	1. (1)	2. (1)	1. (1)
C(21)	1.057 (2)	0.474 (2)	0.799 (2)	5. (2)	3. (2)	8. (2)	0. (1)	2. (1)	2. (1)
C(22)	1.184 (2)	0.487 (2)	0.812 (2)	4. (1)	10. (2)	3. (1)	−1. (1)	1. (1)	−1. (1)
C(23)	1.245 (2)	0.416 (2)	0.767 (2)	4. (1)	7. (2)	4. (1)	1. (1)	2. (1)	1. (1)
C(24)	1.193 (2)	0.331 (2)	0.718 (2)	6. (2)	7. (2)	6. (2)	3. (1)	0. (1)	−4. (2)
C(25)	1.075 (2)	0.318 (2)	0.714 (2)	5. (2)	4. (1)	10. (2)	3. (1)	0. (1)	−4. (1)
C(26)	1.010 (2)	0.387 (2)	0.752 (2)	5. (1)	2. (1)	10. (2)	0. (1)	0. (1)	−1. (1)
C(31)	0.992 (2)	0.818 (2)	1.059 (2)	4. (2)	6. (2)	8. (2)	−2. (1)	1. (1)	−2. (2)
C(41)	1.252 (2)	0.570 (1)	0.872 (2)	3. (1)	3. (1)	8. (2)	0. (1)	0. (1)	−2. (1)
C(51)	0.638 (2)	0.600 (2)	0.927 (2)	3. (1)	5. (2)	7. (2)	0. (1)	−1. (1)	3. (1)
C(52)	0.621 (2)	0.450 (2)	0.833 (2)	6. (1)	4. (2)	7. (2)	0. (1)	0. (1)	−3. (1)
C(61)	0.882 (2)	0.364 (2)	0.746 (2)	4. (2)	4. (2)	15. (3)	2. (1)	−1. (2)	−2. (2)
C(62)	0.682 (2)	0.395 (2)	0.764 (3)	5. (2)	11. (3)	23. (4)	−2. (2)	2. (2)	−12. (3)
C	0.821 (2)	0.630 (3)	0.587 (3)	7. (2)	16. (3)	14. (3)	2. (2)	2. (2)	4. (3)
H(113)	0.820	0.919	1.125	4.8					
H(114)	0.620	0.885	1.111	5.5					
H(115)	0.546	0.736	1.027	4.1					
H(123)	1.329	0.424	0.773	3.6					
H(124)	1.238	0.285	0.683	3.8					
H(125)	1.037	0.260	0.682	4.7					
H(151)	0.558	0.991	0.937	4.3					
H(152)	0.546	0.465	0.791	5.2					
H(252)	0.611	0.407	0.896	5.2					
H(161)	0.857	0.300	0.723	4.0					
H(162)	0.680	0.324	0.789	4.6					
H(262)	0.645	0.402	0.693	4.6					
H(1)O	0.700	0.669	0.676	6.5					
H(1)C	0.905	0.609	0.807	7.0					
H(2)C	0.817	0.691	0.549	7.0					
H(3)C	0.783	0.578	0.534	7.0					
				$Cu(VO)_{0.80}(VO)_{0.20}O_7N_2C_{19}H_{16}$ (2)					
Cu(1)	0.8363 (1)	0.5463 (3)	0.8440 (2)	3.3 (1)	4.18 (10)	10.5 (2)	−0.6 (1)	2.0 (1)	−1.1 (1)
V(1)	1.0390 (2)	0.6806 (2)	0.8949 (3)	4.3 (2)	6.8 (2)	11.8 (4)	−1.0 (2)	2.0 (2)	−4.0 (3)
V(D1)	1.031	0.625	0.959	3.5					
N(5)	0.6844 (8)	0.5386 (8)	0.8767 (9)	4.0 (7)	3.0 (6)	8. (1)	−0.4 (6)	1.4 (7)	−0.9 (7)
N(6)	0.8068 (9)	0.4209 (9)	0.780 (1)	3.6 (8)	6.1 (9)	13. (2)	0.1 (7)	1.6 (9)	−3.3 (10)
O(1)	0.8803 (7)	0.6612 (7)	0.9291 (9)	2.7 (6)	4.7 (6)	11. (1)	0.2 (5)	2.1 (7)	0.1 (7)
O(2)	1.0003 (7)	0.5479 (7)	0.8384 (9)	3.3 (6)	4.5 (6)	13. (1)	−0.6 (5)	2.5 (7)	−4.2 (7)
O(3)	1.0599 (6)	0.7693 (8)	1.0151 (10)	6.2 (8)	7.6 (8)	11. (1)	−1.4 (7)	1.6 (8)	−5.2 (9)
O(4)	1.1979 (7)	0.6363 (7)	0.9171 (8)	3.5 (7)	5.8 (7)	11. (1)	−0.6 (5)	1.2 (7)	−1.1 (7)
O(31)	1.0266 (9)	0.8881 (9)	1.126 (1)	7.0 (9)	10. (1)	14. (1)	−2.5 (8)	2.0 (9)	−7. (1)
O(41)	1.5570 (7)	0.5755 (7)	0.8781 (9)	3.7 (7)	6.5 (8)	11. (1)	−0.7 (6)	1.6 (7)	−0.3 (7)
O	0.7694 (8)	0.6290 (9)	0.6812 (9)	5.5 (8)	10. (1)	9. (1)	1.3 (7)	1.6 (8)	2.5 (9)
O(5)	1.029	0.750	0.791	10. (1)	10. (1)	13. (1)	2.5 (9)	3. (1)	7. (1)
O(D5)	1.061	0.560	1.061	4.5					
C(11)	0.8127 (10)	0.718 (1)	0.980 (1)	3.8 (9)	4.7 (9)	5. (1)	1.2 (7)	0.0 (8)	1.1 (8)
C(12)	0.860 (1)	0.801 (1)	1.041 (1)	5. (1)	4.7 (9)	5. (1)	0.1 (8)	0.0 (9)	0.2 (9)
C(13)	0.788 (1)	0.860 (1)	1.087 (1)	8. (1)	7. (1)	5. (1)	0. (1)	0. (1)	−1. (1)
C(14)	0.673 (1)	0.842 (1)	1.081 (1)	8. (1)	8. (1)	10. (2)	3. (1)	3. (1)	−1. (1)
C(15)	0.626 (1)	0.753 (1)	1.029 (1)	6. (1)	7. (1)	3. (1)	2.1 (9)	−0.4 (9)	1.3 (9)
C(16)	0.6949 (9)	0.692 (1)	0.978 (1)	4.0 (9)	5.6 (9)	5. (1)	1.1 (7)	1.9 (8)	1.4 (9)
C(21)	1.063 (1)	0.4761 (9)	0.803 (1)	4.3 (10)	4.2 (9)	7. (1)	0.6 (7)	2.1 (9)	0.6 (8)
C(22)	1.1843 (9)	0.4882 (9)	0.811 (1)	3.0 (8)	4.6 (8)	4. (1)	0.5 (7)	0.2 (8)	0.2 (8)
C(23)	1.245 (1)	0.417 (1)	0.766 (1)	4.4 (9)	5.3 (10)	8. (1)	0.9 (8)	1.9 (9)	1.0 (9)
C(24)	1.196 (1)	0.333 (1)	0.719 (1)	7. (1)	6. (1)	5. (1)	2. (10)	2. (1)	−0.2 (10)
C(25)	1.074 (1)	0.319 (1)	0.715 (1)	8. (1)	6. (1)	7. (1)	1. (1)	1. (1)	−2. (1)
C(26)	1.006 (1)	0.389 (1)	0.756 (1)	4.2 (10)	4.6 (10)	10. (2)	0.5 (8)	0.5 (10)	−1. (1)
C(31)	0.990 (1)	0.822 (1)	1.062 (1)	7. (1)	7. (1)	9. (1)	−1. (1)	1. (1)	−1. (1)

Table II (*Continued*)

atom	x	y	z	U_{11} or B(A°)	U_{22}	U_{33}	U_{12}	U_{13}	U_{23}
C(41)	1.2517 (10)	0.5694 (10)	0.870 (1)	2.6 (8)	4.8 (9)	8. (1)	1.0 (7)	1.2 (8)	1.0 (9)
C(51)	0.637 (1)	0.601 (1)	0.928 (1)	3.5 (9)	4.8 (9)	7. (1)	−0.4 (8)	0.3 (9)	1.5 (9)
C(52)	0.622 (1)	0.450 (1)	0.834 (1)	5. (1)	6.0 (10)	9. (2)	−3.1 (10)	1. (1)	−1. (1)
C(61)	0.882 (1)	0.366 (1)	0.751 (1)	8. (1)	4.7 (10)	9. (2)	−2.3 (10)	0. (1)	−2. (1)
C(62)	0.685 (1)	0.396 (2)	0.765 (2)	5. (2)	11. (2)	38. (4)	−5. (1)	6. (2)	−11. (3)
C	0.823 (2)	0.625 (2)	0.587 (2)	10. (2)	16. (2)	11. (2)	2. (2)	4. (1)	1. (2)
H(113)	0.820	0.919	1.125	4.8					
H(114)	0.620	0.885	1.111	5.5					
H(115)	0.546	0.736	1.027	4.1					
H(123)	1.329	0.424	0.773	3.6					
H(124)	1.238	0.285	0.683	3.8					
H(125)	1.037	0.260	0.682	4.7					
H(151)	0.558	0.591	0.937	4.3					
H(152)	0.546	0.465	0.791	5.2					
H(252)	0.611	0.407	0.896	5.2					
H(161)	0.857	0.300	0.723	4.0					
H(162)	0.680	0.324	0.789	4.6					
H(262)	0.645	0.402	0.693	4.6					
H(1)O	0.700	0.669	0.676	6.5					
H(1)C	0.905	0.609	0.607	7.0					
H(2)C	0.817	0.691	0.549	7.0					
H(3)C	0.783	0.578	0.534	7.0					
			$CuCu_{0.15}(VO)_{0.85}O_7N_2C_{17}H_{16}$ (3)						
Cu(1)	0.8345 (1)	0.5438 (1)	0.8475 (2)	3.5 (1)	4.0 (1)	8.9 (2)	−0.3 (1)	1.2 (1)	−1.1 (2)
V(1)	1.0425 (3)	0.6731 (5)	0.9069 (7)	3.4 (2)	5.5 (4)	14.2 (5)	−1.0 (2)	2.0 (3)	−3.2 (4)
Cu(2)	1.038	0.642	0.941	4.5					
O(5)	1.032	0.735	0.797	18. (3)	17. (2)	31. (4)	0. (2)	7. (2)	−8. (2)
N(5)	0.6804 (9)	0.539 (1)	0.880 (1)	3.0 (9)	4.4 (9)	7. (1)	−0.4 (9)	−0.6 (9)	2. (1)
N(6)	0.807 (1)	0.419 (1)	0.785 (1)	5. (1)	5.1 (10)	10. (2)	0.5 (9)	1. (1)	−2. (1)
O(1)	0.8806 (8)	0.6579 (7)	0.9326 (9)	3.3 (8)	4.5 (7)	10. (1)	−0.7 (6)	2.7 (8)	−2.3 (8)
O(2)	0.9994 (8)	0.5416 (8)	0.8440 (9)	4.4 (8)	3.6 (7)	12. (1)	−0.4 (7)	1.7 (8)	−3.5 (8)
O(3)	1.0635 (9)	0.7741 (8)	1.0174 (10)	4.6 (9)	7.2 (9)	10. (1)	−0.6 (8)	0.9 (9)	−3.5 (9)
O(4)	1.1986 (8)	0.6355 (7)	0.9193 (9)	3.5 (8)	3.8 (7)	12. (1)	−0.1 (7)	1.0 (8)	−1.5 (8)
O(31)	1.0316 (9)	0.8905 (10)	1.122 (1)	7. (1)	8. (1)	14. (2)	−2.0 (9)	0. (1)	−6. (1)
O(41)	1.3578 (8)	0.5706 (7)	0.8771 (9)	2.9 (8)	5.4 (8)	13. (1)	−0.6 (6)	1.7 (8)	−0.3 (8)
O	0.7734 (9)	0.6256 (9)	0.6816 (9)	5.8 (10)	9. (1)	8. (1)	1.7 (8)	0.9 (9)	2.6 (9)
C(11)	0.816 (1)	0.719 (1)	0.982 (1)	4. (1)	6. (1)	3. (1)	2. (1)	0. (1)	1. (1)
C(12)	0.865 (1)	0.806 (1)	1.041 (1)	4. (1)	3. (1)	7. (2)	−0.2 (10)	0. (1)	−2. (1)
C(13)	0.794 (1)	0.865 (1)	1.083 (1)	8. (2)	4. (1)	9. (2)	1. (1)	1. (1)	−2. (1)
C(14)	0.673 (1)	0.847 (1)	1.075 (2)	6. (2)	7. (1)	10. (2)	2. (1)	1. (1)	−3. (1)
C(15)	0.629 (1)	0.759 (1)	1.028 (1)	4. (1)	8. (1)	4. (2)	1. (1)	1. (1)	0. (1)
C(16)	0.693 (1)	0.693 (1)	0.978 (1)	4. (1)	4. (1)	4. (1)	0.3 (9)	1. (1)	−1. (1)
C(21)	1.062 (1)	0.473 (1)	0.804 (1)	3. (1)	4. (1)	8. (2)	0. (1)	1. (1)	0. (1)
C(22)	1.181 (1)	0.486 (1)	0.812 (1)	4. (1)	3. (1)	7. (2)	0.6 (9)	1. (1)	1.8 (10)
C(23)	1.243 (1)	0.415 (1)	0.766 (1)	5. (1)	7. (1)	4. (2)	2. (1)	0. (1)	0. (1)
C(24)	1.189 (1)	0.325 (1)	0.716 (1)	9. (2)	6. (1)	5. (2)	2. (1)	1. (1)	−2. (1)
C(25)	1.075 (1)	0.311 (1)	0.718 (1)	6. (1)	4. (1)	8. (2)	2. (1)	0. (1)	−2. (1)
C(26)	1.008 (1)	0.385 (1)	0.761 (1)	5. (1)	7. (1)	3. (1)	0. (1)	0. (1)	−1. (1)
C(31)	0.993 (1)	0.826 (1)	1.062 (1)	8. (2)	4. (1)	7. (2)	−1. (1)	1. (1)	−3. (1)
C(41)	1.251 (1)	0.569 (1)	0.872 (1)	4. (1)	4. (1)	7. (2)	0. (1)	1. (1)	2. (1)
C(51)	0.636 (7)	0.604 (1)	0.931 (1)	4. (1)	4. (1)	7. (2)	1. (1)	1. (1)	1. (1)
C(52)	0.620 (1)	0.452 (1)	0.838 (1)	5. (1)	5. (1)	9. (2)	−1. (1)	2. (1)	−3. (1)
C(61)	0.879 (1)	0.361 (1)	0.756 (1)	5. (1)	6. (1)	6. (2)	−1. (1)	−2. (1)	−2. (1)
C(62)	0.679 (2)	0.397 (2)	0.771 (2)	6. (2)	14. (2)	33. (4)	−6. (2)	6. (2)	−15. (3)
C	0.826 (2)	0.620 (2)	0.588 (2)	9. (2)	14. (2)	13. (2)	3. (2)	3. (2)	5. (2)
H(113)	0.822	0.928	1.120	5.0					
H(114)	0.628	0.899	1.113	5.0					
H(115)	0.550	0.745	1.027	5.0					
H(123)	1.327	0.423	0.771	5.0					
H(124)	1.237	0.275	0.687	5.0					
H(125)	1.033	0.256	0.682	5.0					
H(151)	0.558	0.591	0.937	4.3					
H(152)	0.902	0.414	0.895	5.0					
H(252)	0.543	0.476	0.793	5.0					
H(161)	0.857	0.300	0.723	4.0					
H(162)	0.646	0.498	0.689	5.0					
H(262)	0.671	0.327	0.780	5.0					
H(1)O	0.700	0.669	0.676	6.5					
H(1)C	0.905	0.609	0.607	7.0					
H(2)C	0.817	0.691	0.549	7.0					
H(3)C	0.783	0.578	0.534	7.0					

[a] Estimated standard deviations in the last significant figure are given in parentheses. The anisotropic thermal ellipsoid is $\exp[-(\beta_{11}h^2 + \beta_{22}k^2 + \beta_{33}l^2 + 2\beta_{12}hk + 2\beta_{13}hl + 2\beta_{23}kl)]$. The β values are multiplied by 10^4.

ground state. The spectrum exhibits six peaks from 530 to 8000 G, which appear unmodified in the whole temperature range, except a broadening of the peak around 2200 G. It can be interpreted by following the theory of EPR randomly orientated

Table III. Main Bond Lengths and Bond Angles for 1, 2, 3, and 4

	1	2		3		4
	M′ = V(1)	M′ = V(1) with O(5)	M′ = V(D1) with O(5) = O(D5)	M′ = V(1)	M′ = Cu(2)	M′ = Cu(2)
Bond Lengths						
Cu(1)-O(1)	1.912 (9)	1.899 (8)		1.885 (9)		1.924 (3)
Cu(1)-O(2)	1.958 (8)	1.925 (7)		1.924 (8)		1.902 (3)
Cu(1)-N(5)	1.895 (8)	1.889 (8)		1.909 (9)		1.895 (4)
Cu(1)-N(6)	1.878 (9)	1.877 (9)		1.861 (10)		1.907 (4)
Cu(1)-O	2.304 (8)	2.311 (9)		2.312 (10)		2.266 (4)
Cu(1)-Cu(2)				2.763 (2)		2.942 (2)
Cu(1)-V(1)	2.989 (4)	2.949 (3)		2.960 (4)		
Cu(1)-V(D1)		3.507 (3)				
M′-O(1)	2.014 (8)	1.989 (7)	1.79 (1)	1.976 (9)	1.826 (9)	1.919 (3)
M′-O(2)	1.978 (8)	1.962 (8)	1.89 (1)	1.967 (10)	1.805 (10)	1.929 (3)
M′-O(3)	1.901 (9)	1.897 (9)	2.09 (1)	1.911 (11)	2.018 (11)	1.884 (3)
M′-O(4)	1.893 (7)	1.909 (8)	2.11 (1)	1.861 (8)	1.933 (9)	1.873 (3)
M′-O(5)	1.576 (9)	1.586 (4)	1.563 (9)	1.581 (10)		
O(1)-O(2)	2.511 (8)	2.503 (9)		2.478 (13)		2.461 (4)
O(1)-O(3)	2.610 (9)	2.614 (9)		2.688 (13)		2.726 (4)
O(1)-N(5)	2.810 (8)	2.792 (11)		2.798 (14)		2.818 (5)
O(2)-O(4)	2.606 (9)	2.612 (10)		2.647 (13)		2.751 (5)
O(2)-O(6)	2.815 (10)	2.812 (12)		2.767 (16)		2.806 (5)
N(5)-N(6)	2.612 (13)	2.576 (14)		2.620 (19)		2.630 (6)
O(3)-O(4)	2.820 (12)	2.837 (12)		2.857 (15)		2.796 (6)
O-O(1)	3.118 (12)	3.123 (14)		3.134 (15)		3.097 (5)
O-O(2)	3.216 (16)	3.184 (12)		3.189 (14)		3.046 (5)
O-N(5)	3.120 (16)	3.075 (16)		3.086 (16)		3.088 (5)
O-N(6)	3.093 (11)	3.050 (13)		3.066 (14)		3.224 (6)
O-C	1.407 (12)	1.421 (17)		1.403 (10)		1.414 (7)
O(5)-O(1)	2.923 (10)	2.923 (8)		2.848 (9)		
O(5)-O(2)	2.879 (9)	2.841 (9)		2.724 (10)		
O(5)-O(3)	2.740 (11)	2.747 (10)		2.724 (10)		
O(5)-O(4)	2.770 (11)	2.743 (8)		2.692 (9)		
N(5)-C(51)	1.218 (13)	1.260 (14)		1.250 (17)		1.280 (6)
N(5)-C(52)	1.457 (14)	1.458 (14)		1.420 (18)		1.478 (6)
N(6)-C(61)	1.284 (13)	1.271 (15)		1.242 (18)		1.287 (6)
N(6)-C(62)	1.486 (12)	1.438 (16)		1.501 (19)		1.465 (6)
C(52)-C(62)	1.427 (16)	1.426 (19)		1.390 (23)		1.537 (7)
O(1)-C(11)	1.297 (14)	1.343 (13)		1.340 (16)		1.332 (5)
O(2)-C(21)	1.319 (15)	1.332 (12)		1.325 (16)		1.335 (5)
O(3)-C(31)	1.233 (15)	1.300 (15)		1.274 (17)		1.294 (6)
O(4)-C(41)	1.310 (13)	1.303 (13)		1.289 (16)		1.291 (6)
C(51)-C(16)	1.479 (16)	1.478 (18)		1.443 (19)		1.464 (7)
C(61)-C(26)	1.507 (18)	1.468 (17)		1.515 (19)		1.471 (7)
C(31)-C(12)	1.474 (19)	1.507 (16)		1.493 (20)		1.509 (7)
C(41)-C(22)	1.486 (18)	1.465 (17)		1.499 (19)		1.522 (7)
C(31)-O(31)	1.246 (17)	1.220 (15)		1.174 (16)		1.220 (6)
C(41)-O(41)	1.197 (18)	1.219 (11)		1.228 (14)		1.219 (5)
C(11)-C(12)	1.386 (19)	1.405 (17)		1.441 (17)		1.406 (6)
C(12)-C(13)	1.436 (18)	1.367 (16)		1.315 (14)		1.403 (6)
C(13)-C(14)	1.348 (17)	1.348 (19)		1.408 (19)		1.396 (7)
C(14)-C(15)	1.373 (18)	1.421 (20)		1.366 (21)		1.372 (7)
C(15)-C(16)	1.424 (17)	1.388 (17)		1.378 (18)		1.407 (7)
C(16)-C(11)	1.438 (19)	1.409 (14)		1.462 (17)		1.417 (6)
C(21)-C(22)	1.468 (17)	1.410 (14)		1.376 (17)		1.418 (6)
C(22)-C(23)	1.380 (14)	1.377 (17)		1.388 (19)		1.402 (7)
C(23)-C(24)	1.388 (13)	1.355 (12)		1.426 (21)		1.376 (8)
C(24)-C(25)	1.375 (18)	1.413 (18)		1.362 (19)		1.370 (7)
C(25)-C(26)	1.336 (17)	1.392 (18)		1.429 (19)		1.403 (7)
C(26)-C(21)	1.401 (16)	1.417 (17)		1.403 (19)		1.413 (7)
Bond Angles						
N(5)-Cu(1)-O(1)	95.2 (6)	95.1 (4)		95.0 (5)		95.1 (2)
O(1)-Cu(1)-O(2)	80.9 (5)	81.3 (3)		81.2 (4)		80.0 (1)
O(2)-Cu(1)-N(6)	94.4 (6)	95.5 (4)		93.9 (5)		94.9 (2)
N(6)-Cu(1)-N(5)	87.6 (8)	86.5 (5)		88.0 (6)		87.5 (2)
O-Cu(1)-N(5)	93.7 (6)	92.5 (4)		93.5 (4)		95.2 (2)
O-Cu(1)-O(1)	94.9 (6)	95.5 (4)		96.1 (4)		94.9 (2)
O-Cu(1)-O(2)	97.6 (6)	97.5 (4)		97.2 (4)		93.4 (2)
O-Cu(1)-O(6)	94.8 (8)	93.9 (5)		93.9 (5)		100.6 (2)
Cu(1)-O-C	126.0 (9)	124.7 (8)		126.2 (9)		126.7 (2)
Cu(1)-O(1)-M′	98.9 (7)	98.7 (4)	91.9 (4)	100.1 (4)	96.2 (4)	99.9 (1)
Cu(1)-O(2)-M′	98.4 (6)	99.1 (4)	90.8 (4)	99.0 (5)	95.6 (5)	100.3 (1)
O(1)-M′-O(3)	85.0 (6)	84.2 (4)	84.0 (4)	87.5 (4)	88.6 (4)	91.5 (2)
O(3)-M′-O(4)	97.0 (7)	96.3 (4)	85.1 (3)	98.5 (4)	92.6 (4)	96.2 (2)
O(4)-M′-O(2)	85.8 (6)	84.8 (3)	83.3 (3)	87.4 (4)	90.1 (4)	92.7 (2)
O(2)-M′-O(1)	79.7 (5)	78.3 (3)	87.8 (4)	77.9 (4)	86.1 (4)	79.5 (1)
O(5)-M′-O(1)	106.1 (7)	109.0 (3)	112.7 (3)	105.9 (4)		
O(5)-M′-O(3)	105.2 (9)	104.0 (4)	105.5 (4)	102.1 (5)		
O(5)-M′-O(4)	100.4 (9)	102.8 (3)	100.1 (4)	97.4 (5)		
O(5)-M′-O(2)	102.3 (8)	106.3 (3)	109.5 (3)	99.8 (4)		

Table IV. Mean Planes

Mean Planes[a]

A defined by O(1)O(2)N(5)N(6)
B defined by O(1)O(2)O(3)O(4)
C defined by OCu(1)M'
D defined by Cu(1)M'O(5)
E defined by Cu(1)OC

Dihedral Angles[b]

	1	2	3	4		1	2	3	4
A–B	190.3	190.1	187.6	191.6	B–D	90.5	91.1	93.9	
A–C	91.6	91.1	90.5	91.4	C–D	3.5	3.8	5.7	
A–D	88.0	87.4	84.8		E–C	73.7	71.3	72.0	55.9
B–C	92.9	92.6	92.0	98.0					

Deviation of the Atoms from Mean Planes[c]

	A				B				C				D		
atoms	1	2	3	4	1	2	3	4	1	2	3	4	1	2	3
Cu(1)	176	161	169	204	−83	−85	−17	−70	0	0	0	0	0	0	0
Cu(2)			−372	−318			−203	−30			−2	0			−57
V(1)	174	257	176		436	512	373		0	0	0		0	0	0
V(D1)		−758				−567				56				−10	
O(1)	6	6	8	−61	−27	−19	−18	23	1258	1263	1230	1237	1247	1239	1209
O(2)	−6	−6	−9	54	33	22	20	−18	−1241	−1233	−1248	−1225	−1252	−1247	−1261
O(3)	−399	−398	−301	−632	23	16	15	−19	1479	1460	1477	1407	1444	1413	1423
O(4)	−529	−493	−390	−427	−28	−19	−17	15	−1341	−1378	−1377	−1338	−1384	−1429	−1429
N(5)	−6	−6	−8	62	−537	−509	−398	−387	1303	1290	1313	1318	1291	1281	1290
N(6)	5	6	8	−49	−453	−445	−320	−658	−1322	−1293	−1306	−1309	−1332	−1299	−1316
O	2491	2469	2480	2468	2186	2172	2262	2173	0	0	0	0	141	153	230
C	3347	3319	3331	3306	3110	3089	3169		−1116	−1111	−1077		−923	−902	−758
O(5)	1835	1800	1726		2142	2095	1948		−101	−101	−165		0	0	0
O(D5)		−2272				−2085				38				−127	

[a] M' = V(1) in **1**, **2**, and **3**, Cu(2) in 4. [b] In degrees. [c] Distances × 10^3 in angstroms.

triplet states given by Wasserman et al.[24] The case of pairs of nonequivalent spin doublets was approached by Care et al. with a specific emphasis to the Cu^{II}–VO^{II} system.[25]

From the analysis of the spectrum, the presence of six features, and especially the dissymmetry in their position, it can be deduced that the ground state is actually a triplet state with rhombic g and D tensors, implying for the zero-field splitting parameters values necessarily less than the value of the incident quantum $h\nu \simeq 0.3$ cm^{-1}. An attempt of quantitative interpretation was performed from the Hamiltonian, $\mathcal{H} = \beta\vec{H}(g)\hat{S} + \hat{S}(D)\hat{S}$, with $S = 1$, and Wasserman's equation:[24]

$$H_{x_1}^2 = (g_e/g_x)^2[(H_0 - D' + E')(H_0 + 2E')]$$

$$H_{x_2}^2 = (g_e/g_x)^2[(H_0 + D' - E')(H_0 - 2E')]$$

$$H_{y_1}^2 = (g_e/g_y)^2[(H_0 - D' - E')(H_0 - 2E')]$$

$$H_{y_2}^2 = (g_e/g_y)^2[(H_0 + D' + E')(H_0 + 2E')]$$

$$H_{z_1}^2 = (g_e/g_z)^2[(H_0 - D')^2 - E'^2]$$

$$H_{z_2}^2 = (g_e/g_z)^2[(H_0 + D')^2 - E'^2]$$

with

$$H_0 = h\nu/(g_e\beta)$$

$$D' = D/(g_e\beta)$$

$$E' = E/(g_e\beta)$$

In fact, this quantitative approach was proving difficult. Indeed, the peaks are large, and the magnetic fields corresponding to the resonances cannot be determined accurately. In other respects, attempted determination of a univocal set of five parameters (g_x, g_y, g_z, D, and E) from six experimental data, namely the six fields H_{u_i} ($u = x$, y, and z; $i = 1$ and 2), using the usual least-squares procedure, is clearly not an easy task. Furthermore, in Wasserman's equations given above, it is assumed that the D and g tensor axes are coincident. This could not be the case for an heterobinuclear complex. Concretely, we have not been able to determine the principal values of the g tensor. On the other hand, for all the sets of parameters leading to a satisfying theory–experiment agreement, $|D|$ and E take values around 0.24 cm^{-1} and 0.04 cm^{-1}, respectively. The average g value is then surprisingly around 1.8. It must be pointed out that, from these values, the resonant field H_{min} associated with the $\Delta M_S = 2$ transition is expected at a value very close to H_{z_1}. This provides an explanation for the intensity of the first peak with regard to the others and confirms the reliability of our EPR data interpretation.

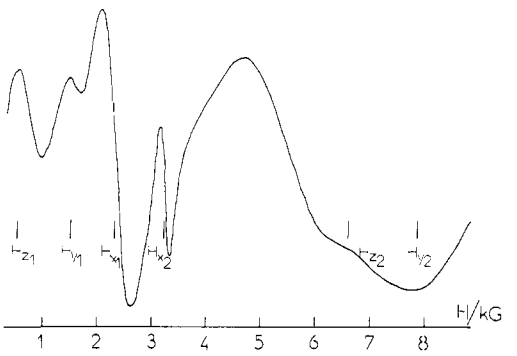

Figure 6. X-band powder EPR spectrum of **1** at 100 K.

Mechanism of the Ferromagnetic Coupling of the Cu^{II}–VO^{II} Pairs

We purpose to present this part devoted to the mechanism of the interaction in $CuVO(fsa)_2en\cdot CH_3OH$ in two stages. In the first stage, we shall show that the observed ferromagnetic coupling may be explained very simply by considering the relative symmetries of the magnetic orbitals ϕ_{Cu} and ϕ_{VO}. This will be done briefly since most of the elements of the discussion had been given in ref 2. In the second step, we shall refine our investigation and justify the magnitude of the interaction. In some way, we purpose to investigate the mechanism of the interaction, first with weakly magnifying glasses, only able to specify the symmetries of the magnetic orbitals, and then with strongly magnifying glasses,

(24) Wasserman, E.; Synder L. C.; Yager, W. A. *J. Chem. Phys.* **1964**, *41*, 1763–1772.
(25) Carr, S. G.; Smith, T. D.; Pilbrow, J. R. *J. Chem. Soc., Faraday Trans. 2* **1974**, *70*, 497–511.

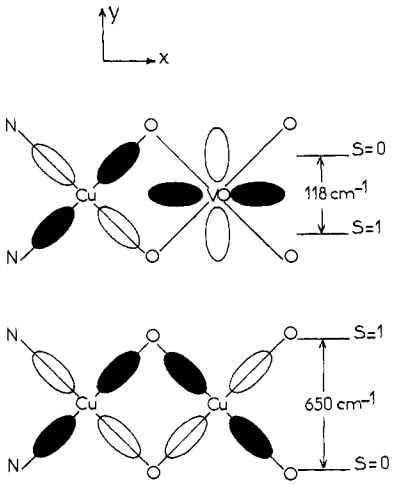

Figure 7. Relative symmetries of the magnetic orbitals in CuVO-(fsa)$_2$en·CH$_3$OH and Cu$_2$(fsa)$_2$en·CH$_3$OH.

giving much more detail on the magnitude of the magnetic orbitals in any point of the space.

We have seen in the structural part that the oxygen atoms of both the vanadyl group and the methanol molecule and the copper and vanadium atoms formed a mirror plane for the CuN_2O_3 and VO_5 square pyramids. It turns out that the symmetries of the metallic sites and the whole molecular symmetry are very close to C_s. The magnetic orbital ϕ_{Cu} centered on a Cu^{II} ion in a 4 + 1 environment is constructed from the d_{xy} metallic orbital and partially delocalized toward the oxygen and nitrogen atoms surrounding the copper owing to the σ-type antibonding overlaps $\langle d_{xy}|p_\sigma\rangle$. This magnetic orbital is therefore antisymmetric with regard to the CuOVO mirror plane. It transforms as the a'' irreducible representation of the C_s group. The magnetic orbital ϕ_{VO} is constructed from the $d_{x^2-y^2}$ metallic orbital and is partially delocalized toward the oxygen atoms of the pseudomolecular plane owing to the π-type antibonding overlaps $\langle d_{x^2-y^2}|p_\pi\rangle$. That magnetic orbital is symmetric with regard to the mirror plane; it transforms as a'. Thus, the overlap integral $\langle\phi_{Cu}|\phi_{VO}\rangle$ is identically zero. There is no interaction between ϕ_{Cu} and ϕ_{VO} favoring the pairing of the electrons on a molecular orbital of low energy. If one expresses the triplet–singlet energy gap J according to

$$J = J_{AF} + J_F$$

where J_{AF} is the negative antiferromagnetic contribution favoring the pairing of the electrons and related in absolute value to the overlap between the magnetic orbitals and J_F, the positive ferromagnetic contribution defined as

$$J_F = 2\langle\phi_{Cu}(1)\phi_{VO}(2)|r_{12}^{-1}|\phi_{Cu}(2)\phi_{VO}(1)\rangle$$

then one has in the Cu^{II}–VO^{II} complex

$$J = J_F$$

The coupling is purely ferromagnetic, and the spin triplet is the ground level. This situation of strict orthogonality of the magnetic orbitals is schematized in Figure 7 and compared to the situation encountered in Cu$_2$(fsa)$_2$en·CH$_3$OH. In this latter complex, the two magnetic orbitals have the same a″ symmetry. The CuOCu bridging angle is equal to 100.2°. It is therefore larger than the very peculiar value close to 90°, for which an *accidental orthogonality* of the magnetic orbitals could be expected. In fact, the intramolecular interaction in Cu$_2$(fsa)$_2$en·CH$_3$OH is strongly antiferromagnetic, the $S = 0$ level being 650 cm^{-1} lower in energy than the $S = 1$ level.

If the orthogonality of the magnetic orbitals as shown in Figure 7 explains why the interaction in CuVO(fsa)$_2$en·CH$_3$OH is ferromagnetic, it does not explain why J is found to be so large. To understand the magnitude of the interaction, we must examine more closely the relative orientations of ϕ_{Cu} and ϕ_{VO}. These two

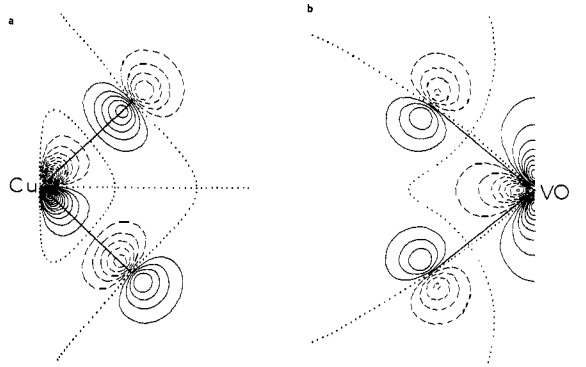

Figure 8. (a) Magnetic orbital ϕ_{Cu}. (b) Magnetic orbital ϕ_{VO}. The solid lines represent the positive isovalue curves and the dashed lines the negative ones. The dotted lines represent the nodal zones.

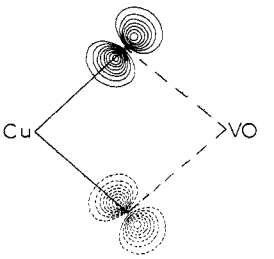

Figure 9. Overlap density map in **1**. The solid lines represent the positive isooverlap density curves and the dashed lines the negative ones. The dotted lines represent the nodal zones. The differences of overlap density between two successive curves are equal.

magnetic orbitals, as obtained by extended Hückel calculations on the monomeric fragments,[26] are represented in Figure 8. Comparing ϕ_{Cu} and ϕ_{VO}, one notices, in addition to their orthogonality, that the same 2p orbitals of the oxygen bridging atoms occur in ϕ_{Cu}, giving a σ overlap with d_{xy} centered on copper, and in ϕ_{VO}, giving a π overlap with $d_{x^2-y^2}$ centered on vanadium. It turns out that the overlap density defined as

$$\rho = \phi_{Cu}\phi_{VO}$$

presents two strongly positive lobes around one of the bridges along the CuO axis and two strongly negative lobes around the other bridge.[27] Figure 9 gives the overlap density map for the Cu^{II}–VO^{II} pair, plotted in the CuOO plane. Since the depth of the negative lobes (or holes) exactly compensates the altitude of the positive lobes (or summits) one has actually

$$S = \int_{space}\rho(1)\,d\tau(1) \equiv 0$$

On the other hand, the two-electron exchange integral C defined as

$$C = \int\int_{space}\frac{\rho(1)\rho(2)}{r_{12}}\,d\tau(1)\,d\tau(2)$$

the magnitude of which is essentially related to the extrema of ρ, summits or holes, may be important and J may be as large as 118 cm^{-1}. Our approach makes the important point, generally overlooked in discussions of exchange interaction in solids, that

(26) To obtain ϕ_{Cu} and ϕ_{VO}, we use the FORTICON8 version of the EH method with charge iteration on all atoms and Madelung correction. The monomeric fragments we consider were actually $(NH_3)_2CuX_2$ and $X_2VO(NH_3)_2$, X being an element of the first row of the periodic chart. The details on the choice of the atomic orbitals and on the value of the parameters of the method were given in ref 27.

(27) Kahn, O.; Charlot, M. F. *Nouv. J. Chim.* **1980**, *4*, 567–576. "Quantum Theory of Chemical Reactions"; Reidel (Dordrecht): Netherlands, 1980; Vol. II, pp 215–240.

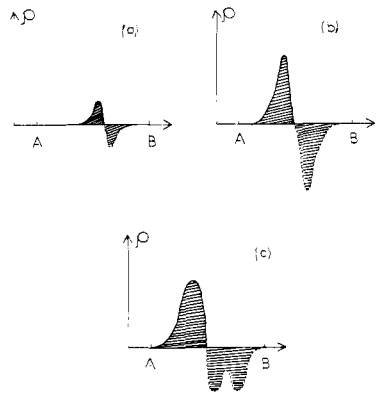

Figure 10. Variation of the overlap density in the three cases of orthogonality of the magnetic orbitals: (a) strict orthogonality and weak ferromagnetic interaction; (b) strict orthogonality and strong ferromagnetic interaction; (c) accidental orthogonality (see text).

the entire molecular symmetry is important in deciding the nature of the coupling and not only the local symmetry for each A–O–B linkage. In the Cu^{II}–VO^{II} pair, the strict orthogonality which leads to ferromagnetic interaction occurs only if the phases at both bridging oxygen atoms are taken into account. Ignoring these phases, we could obtain the erroneous conclusion that along each CuOV linkage, the $d_{xy}\|p\|d_{x^2-y^2}$ pathway gives antiparallel coupling, hence that the interaction should be strongly antiferromagnetic.

In a more general way, in any coupled system where the orthogonality of the magnetic orbitals is realized, the magnitude of the interaction may be estimated from such considerations of overlap densities, as schematized in Figure 10. The cases a and b correspond to a real orthogonality related to the symmetry properties of the complex and of the magnetic orbitals. In case a, the overlap density presents itself in the form of a hill of weak altitude close to a shallow pond. In case b, it presents itself in the form of a very high montain close to a very deep sea. One sees clearly that case a is associated with a weak ferromagnetic interaction and b with a strong ferromagnetic interaction. For completeness, we joined to Figure 10 case c, corresponding to an *accidental orthogonality*, not directly related to the symmetry properties of the problem. For very peculiar values of the structural parameters, which cannot be known exactly a priori, the depth of the two ponds compensates the altitude of the unique summit so that $\int_{space}\rho(1)d\tau(1)$ is equal to zero. Any structural deformation will destroy this accidental orthogonality, even if it does not change the molecular symmetry group. A nice example of accidental orthogonality is obtained in the planar hydroxo-bridged copper(II) dimers extensively studied by Hatfield and Hodgson.[28]

Strategy and Conclusion

We have seen why the pair Cu^{II}–VO^{II} with the symmetry imposed by the nature of the binucleating ligand $(fsa)_2en^{4-}$ was particularly well adapted to give rise to a strong ferromagnetic coupling. In this last part, we look for other pairs which could be used to obtain again a strong stabilization of the level of highest spin multiplicity with the same ligand.

The five possible types of magnetic orbitals with their symmetry in O_h, C_{2v}, and C_s groups are represented in Figure 11. Table V specifies the nature and the magnitude of the interaction for each couple of magnetic orbitals.

Let us consider first that one of the sites is occupied by a metallic ion with an unpaired electron in a (x^2-y^2)-type magnetic orbital. The interaction with another x^2-y^2 orbital will have an indirect component through the bridges and also a nonnegligible direct metal–metal component due to the relative orientations of the $d_{x^2-y^2}$ metallic orbitals. The former component will vary from the strong antiferromagnetism for AOB bridging angles much

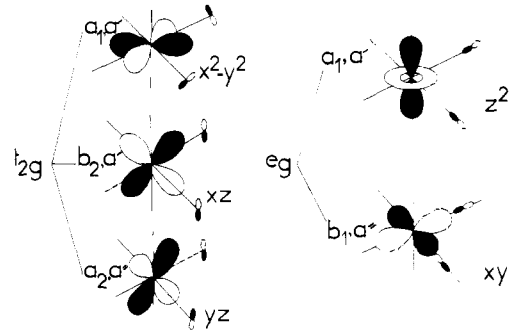

Figure 11. Schematic representation and symmetry of the magnetic orbitals in O_h, C_{2v}, and C_s (see text).

Table V. Predicted Nature and Magnitude of the Interaction between Pairs of Magnetic Orbitals

	x^2-y^2	xz	yz	z^2	xy
x^2-y^2	from a to A	f	f	a	F
xz		a	from f to F	f	f
yz			a	f	f
z^2				from a to F	f
xy					from A to F

[a] a = weakly antiferromagnetic; A = strongly antiferromagnetic; f = weakly ferromagnetic; F = strongly ferromagnetic (see text).

larger than 90° to the ferromagnetism due to an accidental zero value of the overlap density around each bridge for bridging angles close to 90°. The latter component is always antiferromagnetic and increases when the A–B metal–metal distance decreases, hence when the bridging angle decreases. For bridging angles close to 90°, the direct component should dominate so that the $x^2-y^2 \leftrightarrow x^2-y^2$ interaction should vary from strong antiferromagnetism (A) to weak antiferromagnetism (a). The interactions $x^2-y^2 \leftrightarrow xz$ and $x^2-y^2 \leftrightarrow yz$ between orthogonal magnetic orbitals are weakly ferromagnetic (f), since the overlap density around each bridge is weak. The $x^2-y^2 \leftrightarrow z^2$ interaction should be rather weakly antiferromagnetic. Indeed, the p orbitals of the bridges occurring in the magnetic orbitals have the proper orientations to give rise to zones of important in-phase overlap density around each bridge. However the spin density on the bridges in z^2 is weak owing to the preferential orientation of the metallic d_{z^2} orbital along the axis perpendicular to the pseudomolecular plane. As for the $x^2-y^2 \leftrightarrow xy$ interaction, we have seen that it was strongly ferromagnetic (F).

Let us consider now the second line of Table V where one of the sites has an unpaired electron in xz. This magnetic orbital is generally weakly delocalized toward the bridging atoms so that $xz \leftrightarrow xz$ will be weakly antiferromagnetic and $xz \leftrightarrow yz$, $xz \leftrightarrow z^2$, and $xz \leftrightarrow xy$ will be weakly ferromagnetic. If the bridging atoms become less electronegative (nitrogen or sulfur atoms for instance), the delocalization of xz and yz may be more important and the $xz \leftrightarrow yz$ interaction become more strongly ferromagnetic with for the overlap density two positive lobes around one of the bridges on both sides of the molecular plane and two negative lobes around the other bridge.

As far as the third line of Table V is concerned, arguments of the same kind as above allow one to expect a weak antiferromagnetic interaction for $yz \leftrightarrow yz$ and weak ferromagnetic interactions for $yz \leftrightarrow z^2$ and $yz \leftrightarrow xy$.

We have seen that the z^2 magnetic orbital is weakly delocalized toward the ligands located in the pseudomolecular plane. It turns out that $z^2 \leftrightarrow z^2$ will be weak in magnitude but will depend on the nature of the AOB bridging angles. An accidental orthogonality may be obtained for bridging angles close to 90°. The $z^2 \leftrightarrow xy$ is clearly weakly ferromagnetic. Finally, the $xy \leftrightarrow xy$ interaction may be strong in magnitude owing to the importance of the delocalization of the magnetic orbitals toward the bridges. An accidental orthogonality may be again expected, and is ex-

(28) Crawford, V. H.; Richardson, H. W.; Wasson, J. R.; Hodgson, D. J.; Hatfield, W. E. *Inorg. Chem.* **1976**, *15*, 2107–2110.

perimentally observed,[28] for bridging angles close to 90°.

Examining Table V, one can notice that the F situation related to the real orthogonality of the magnetic orbitals is exceptional. It only occurs in the $x^2 - y^2 \leftrightarrow xy$ interaction, as found in Cu^{II}–VO^{II} and also in low-spin Co^{II}–Cu^{II}. In this latter case, unfortunately, we have not been able to grow single crystals, so that the structure of the complex is not known with accuracy.[29] There is one new pair of A–B ions with a pure ferromagnetic coupling, and apparently only one, namely the d^9–d^3 pair in which the magnetic orbitals are xy and $x^2 - y^2$, xz and yz, respectively. In the quite near future, we expect to be able to describe a Cu^{II}–Cr^{III} complex corresponding to this situation.[30]

Registry No. 1, 80765-14-6; $CuH_2(fsa)_2en$, 59229-83-3; $VO(CH_3CO-O)_2$, 3473-84-5; $VO(OH)_2$, 30486-37-4.

Supplementary Material Available: A listing of structure factor amplitudes (23 pages). Ordering information is given on any current masthead page.

(29) Kahn, O.; Claude, R.; Coudanne, H. *Nouv. J. Chim.* **1980**, *4*, 167–172.

(30) Journaux, Y.; Kahn, O.; Coudanne, H. *Angew. Chem., Int. Ed. Engl.*, in press.

Kinetic Acidity of Diastereotopic Protons in Sulfonium Ions. 2. Thiolanium Cations. X-ray Molecular Structure of 8-Methyl-8-thioniabicyclo[4.3.0]nonane Tetrafluoroborate and Quantitative Perturbational Molecular Orbital Analysis of Diastereomeric Model Sulfonium Ylides

Giovanni Dario Andreetti,[1a] Fernando Bernardi,[1b] Andrea Bottoni,[1c] and Antonino Fava*[1c]

Contribution from the Istituto di Chimica Organica and Istituto Chimico G. Ciamician, Università di Bologna, 40136 Bologna, Italy, and Istituto di Strutturistica Chimica, Università di Parma, Parma, Italy. *Received August 3, 1981*

Abstract: The X-ray molecular structure has been determined for the title compound **2**, a rigid sulfonium salt which is known[3b,9e] to exchange its α protons with high stereoselectivity. The geometry thus obtained has been utilized to compute by ab initio SCF MO methods the relative stabilities of the $^-CH_2$-SH_2^+ model ylide in the various geometrical arrangements corresponding to the diastereomeric ylides arising from **2** by removal of the α protons one at a time. The computed trend of ylide stability appears to largely match the trend of kinetic acidity, indicating the model is a suitable one. A quantitative PMO analysis[10] has been carried out, allowing for the estimation of the relative energy effects associated with the various orbital interactions. Contrary to recent suggestions,[8,24a] the lone-pair destabilizing interaction never becomes dominant, while the hyperconjugative effect associated to the n_c–σ^*_{SH} interaction appears to play a major conformational role, in agreement with a previous proposal.[6]

Tricoordinated organic sulfur functions Z–S(X)–CH_2R (Z = R, Ar, OR, ...; X = O, OR, R′, NR, Ar′, ...) are pyramidal and configurationally stable. Therefore, whenever X ≠ Z, the methylene protons are diastereotopic and have different reactivity.[2] As these functions are strongly acid enhancing, a conspicous chemical manifestation of this phenomenon is provided by the differential kinetic acidity (base-catalyzed H–D exchange) of the α-CH_2 protons which in a number of cases has been found to reach very high values, ranging into the thousands.[3]

Although the phenomenon is important theoretically, in relation to the general problem of reaction stereospecificity, and practically, in view of a rational approach to the transfer of chirality from sulfur to carbon,[4] the fundamental geometrical factors presiding over it are not clear. To the extent that the transition states for base-catalyzed H–D exchange resembles the carbanionic intermediate, the question of the differential kinetic acidity may be approached in terms of the relative stability of the diastereomeric carbanions (or ylides, as the case may be) arising from the removal of the corresponding diastereotopic protons one at a time.[5] We adopted[6] this approach in an attempt to rationalize the following observations in the *rigid S*-methylthianium cations **1e** and **1a**—in the former, the equatorial α proton is considerably more reactive than its geminal axial companion, while, in the latter, the two protons are about equally reactive.[6]

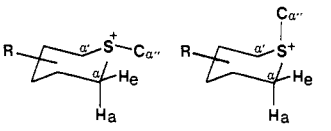

1e $k_e > k_a$ **1a** $k_e > k_a$

If the ylide is a suitable model for the transition state of the base-catalyzed H–D exchange, these results appeared to be consistent with the idea, which emerged in the mid 70's,[7] that the

(1) (a) Istituto di Chimica Organica. (b) Istituto Chimico "G. Ciamician". (c) Istituto di Strutturistica Chimica.

(2) Rauk, A.; Buncel, E.; Moir, R. T.; Wolfe, S. *J. Am. Chem. Soc.* **1965**, *87*, 5498.

(3) (a) Fraser, R. R.; Schuber, F. J.; Wigfield, Y. Y. *J. Am. Chem. Soc.* **1972**, *94*, 8794. (b) Barbarella, G.; Garbesi, A.; Fava, A. *Ibid.* **1975**, *97*, 5883.

(4) Annunziata, R.; Cinquini, M.; Cozzi, F. *J. Chem. Soc., Perkin Trans. 1* **1981**, 1109. Cinquini, M.; Colonna, S.; Maia, A., *Chim. Ind. (Milan)* **1980**, *62*, 859 and references therein.

(5) This approach is obviously limited since it does not account for solvent and salt effects. These are known to be quite large in the case of sulfoxides;[3a] no evidence is available for similar effects in sulfonium salts.[3b] However, medium effects are likely to be small here (compared to sulfoxides), and, especially in aqueous media, the carbanion intermediates closely approximate free ylides.

(6) Barbarella, G.; Dembech, P.; Garbesi, A.; Bernardi, F.; Bottoni, A.; Fava, A. *J. Am. Chem. Soc.* **1978**, *100*, 200.

(7) (a) Lehn, J. M.; Wipff, G. *J. Am. Chem. Soc.* **1976**, *98*, 7498. (b) Epiotis, N. D.; Yates, R. L.; Bernardi, F.; Wolfe, S. *Ibid.* **1976**, *98*, 5435. (c) Bernardi, F.; Schlegel, H. B.; Whangbo, M. H.; Wolfe, S. *ibid.* **1977**, 99, 5633. (d) Epiotis, N. D.; Cherry, W. R.; Shaik, S.; Yates, R. L.; Bernardi, F. *Top. Curr. Chem.* **1977**, *70*.

0002-7863/82/1504-2176$01.25/0